We are IntechOpen,
the world's leading publisher of
Open Access books
Built by scientists, for scientists

4,800
Open access books available

122,000
International authors and editors

135M
Downloads

Our authors are among the

154
Countries delivered to

TOP 1%
most cited scientists

12.2%
Contributors from top 500 universities

CLARIVATE ANALYTICS
BOOK CITATION INDEX
INDEXED

WEB OF SCIENCE™

Selection of our books indexed in the Book Citation Index
in Web of Science™ Core Collection (BKCI)

Interested in publishing with us?
Contact book.department@intechopen.com

Numbers displayed above are based on latest data collected.
For more information visit www.intechopen.com

Semi-Deterministic Single Interaction MIMO Channel Model

Arghavan Emami-Forooshani[1] and Sima Noghanian[2]
[1]University of British Columbia,
[2]University of North Dakota
[1]Canada,
[2]USA

1. Introduction

In systems which employ spatial filtering, Multiple Input Multiple Output (MIMO) systems, switched beam systems or adaptive antennas, distribution of the multipath components is important in determining the performance of the channel [Liberty & Rappaport, 1999], [Allen & Ghavami, 2005]. In this regard, intensive research efforts have been invested. Different measurement campaigns [Ranvier et al., 2007], [Chizhik et al., 2003], [Howard et al., 2002] and site specific propagation prediction methods [Seidel & Rappaport, 1994], [Anderson & Rappaport, 2004], [Gesbert et al., 2002] have been realized to characterize the wireless channel. However, to simulate these systems without using measured data or site specific propagation prediction techniques, a model must be used to generate multipath channel parameters. Therefore, a number of realistic spatial channel models are introduced and the defining equations (or geometry) are described in [Liberty & Rappaport, 1999]. However, these models are only valid for particular environments with specific assumptions. Most of these simple geometrical models such as Lee's and Geometrically-Based Single-Bounce Circular Model (GBSBC) models are only applicable to outdoor environments. In some of these models for instance, it is assumed that the transmitter (Tx) and receiver (Rx) heights are the same which is a reasonable assumption only for some outdoor applications where the Tx and Rx distance is quite large. Moreover, in these simple models scatterers' distribution is restricted into limited areas and the impact of channel (including scatterers) on changing the polarization of the electric field and also antenna pattern effect are not taken into account.

Therefore, there is a need for a general and more accurate model that is valid for both outdoor and indoor environments with different scatterers' distributions. Also a model that includes effects of changing the electric field polarization and antenna characteristics on the channel is required to make realistic conclusions about different environments.

Although ray-tracing may seem as another alternative that is more accurate in terms of scattering environment and antenna characteristics, it is site specific, i.e. it needs exact information about the study area and it is computationally intensive, needing very long runtime. If general conclusions about system configuration based on statistics of the channel are required, ray-tracing may not be a right choice as it demands to change the channel

parameters several times and evaluate and compare the results for many runs. This can be very time consuming if the runtime is too long.

In this chapter a method is introduced that can be used for channel estimation in both indoor and outdoor envrionments. The method is called Single Interaction ScaTEring Reflecting (SISTER) model [Emami, 2010]. This model is based on the method proposed in [Svantesson, 2001]. In that work, a spatio-temporal channel model for MIMO systems is proposed which is based on electromagnetic scattering and wave propagation. By studying the scattering properties of objects of simple shapes, such as spheres and cylinders, a simple function that captures the most important scattering properties is derived. A compact formulation is obtained by using a dyad notation and concepts from rough surface scattering. That model exploits the concept of positioning scattering objects and calculating the received signal including polarization properties of the channel and the antennas and 3-D wave propagation. However, it only accounts for uniformly distributed scatterers in the surrounding environment and does not include different distributions for the scatterers, reflection from the ground and antenna array factor in channel complex impulse response calculations. Moreover, it is not suitable for indoor applications since it does not take into account the reflections from the walls.

The SISTER model was developed to overcome the shortcomings of previous models mentioned above. To keep it simple, spherical shape is chosen for scatterers in order to obtain analytical expressions for scattered fields and only single interaction from each scatterer (or reflector) is considered and the interactions between scatterers (or reflectors) are neglected. Single bounce interaction has been used in some MIMO channel models such as GBSBC and Geometrical Based Single Bounce Macrocell (GBSBM) channel models [Seidel & Rappaport, 1994] and ray-tracing models [Liberty & Rappaport, 1996]. While in reality multiple interactions do exists, the level of interaction strongly depends on type propagation environment. According to [Almers et al., 2007] for picocells, propagation within a single large room is mainly determined by Line-of-Sight (LOS) propagation and single bounce reflections. However if the Tx and Rx are in different rooms, then the radio waves either propagate through the walls or they will be diffracted into the room with the Rx. The multiple-bounce can be accounted using virtual single-bounce scatterers whose position and path-loss are chosen such that they mimic multiple bounce contribution. With this approach SISTER model can be utilized for environments with significant multiple bounce propagation.

The SISTER model not only is general in terms of different fading channels and antenna configuration but also is simple and can run in a reasonable computation time. In SISTER model, scatterers are located in an enclosed area containing Tx and Rx which can have optional distance and heights. Any numbers and distributions including uniform and cluster forms can be defined for scatterers. To increase the accuracy of the model, in addition to scattering, reflections (from the ground for outdoors and from the walls for indoors) are also included in it.

2. Summarized description of the SISTER model

In SISTER model different locations, configurations, radiation patterns and polarizations can be defined for Tx and Rx antennas. Scatterers' distribution, material and size can also be defined. Simple shape of sphere is chosen for scatterers in order to obtain analytical expressions for scattered fields.

This model can be used for both indoor and outdoor applications and there is no limitation on Tx and Rx heights, separation (as long as they are in each others far field) and element spacing. In addition, both Line-of-Sight (LOS) and Non-Line-of-Sight (NLOS) cases are modeled.

Without losing the generality, it is assumed that the Mobile Station (MS) is the transmitter and the Base Station (BS) is the receiver. Therefore, the electric waves are generated at the MS and then propagate towards the scatterers (or reflectors) and finally scatter (or reflect) towards the BS. In order to use far field expressions for antennas, scatterers are located in the far field of both Tx and Rx. From antenna theory, if the distance between the antenna and the object is $r \geq \dfrac{2D^2}{\lambda}$ where D is the largest dimension of the corresponding antenna and λ is the wavelength, object is located in the far_field.

As mentioned earlier, to keep this model simple, only single interaction from each scatterer (or reflector) is considered and the interactions between scatterers (or reflectors) are neglected (Fig. 1).
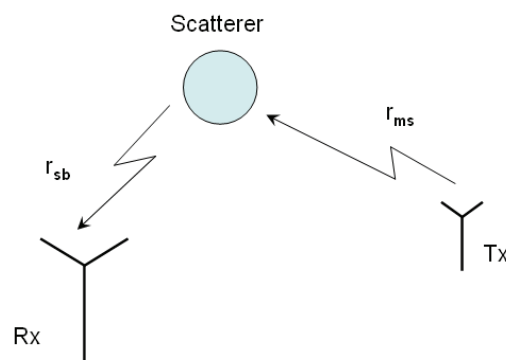

Fig. 1. Single interaction for each scatterer is considered; r_{sb} and r_{ms} are Rx and Tx distances to the scatterer, respectively.

3. Analytical calculations

In this section, different required calculations will be explained first. Then it will be shown how these calculations are used to compute the channel complex impulse response matrix (**H**-matrix) and the channel capacity. By considering an $N_T \times N_R$ -MIMO system, where N_T is the number of transmitters and N_R is the number of receivers, **H**-matrix will consist of $N_T \times N_R$ entries each of which corresponds to a different channel:

$$\mathbf{H}=\begin{bmatrix} h_{11} & h_{12} & h_{11} & h_{11} \\ h_{21} & h_{11} & h_{11} & h_{11} \\ h_{11} & h_{11} & h_{11} & h_{11} \\ h_{11} & h_{11} & h_{11} & h_{11} \end{bmatrix}_{N_T \times N_R} \tag{1}$$

where h_{ij} is the channel impulse response between i^{th} Tx and j^{th} Rx antennas.

Here, two cases of space and angle diversity are considered for the analysis. For space diversity, multiple antennas and for angle diversity, multiple simultaneous beams are assumed at both Tx and Rx.

To calculate each entry of the channel complex impulse response matrix, h_{ij}, first radiated electric field from the first Tx antenna (or beam) which is received by the first scatterer should be calculated. After that, scattered field from the scatterers which is received by the first Rx antenna (or beam) should be calculated. This procedure should be repeated for all scatterers, antennas and beams. The scattered fields then should be summed over all the scatterers at the receiver. Reflected field also should be calculated and added to the resultant field. In the LOS case, electric field for direct path between Tx and Rx should also be included in the summation.

3.1 Transmitter and receiver antenna pattern calculation

To calculate channel complex impulse response, electric field of the antenna elements used at both ends and array factor in case of using the arrays are needed. In order to take mutual coupling into account for the array case, array radiation pattern should be found by full wave analysis using one of antenna design software tools. However, for the sake of simplicity mutual coupling is not considered here. The SISTER model can be applied to different antenna patterns but for convenience, the antenna pattern which is presented here is for a half-wavelength dipole antenna.

Electric field of a *z*-directed half-wavelength dipole antenna is as follows [Balanis, 1997], [Allen & Ghavami, 2005]:

$$E_\theta = j\eta \frac{I_0 e^{-jkr}}{2\pi r} \left[\frac{\cos\left(\frac{\pi}{2}\cos\theta\right)}{\sin\theta} \right] \tag{2}$$

where $E_\theta, \eta, I_0, \theta$ and r are electric field in $\vec{a}_\theta$ direction, intrinsic impedance of free space, current amplitude, elevation angle and radial distance of observation point. Assuming that the array axis is in *z* direction, array factor formula can be obtained by [Balanis, 1997], [Allen & Ghavami, 2005]:

$$\begin{cases} AF = \sum_{n=1}^{N} e^{j(n-1)\Psi} \\ \Psi = kd\cos\theta + \beta \end{cases} \tag{3}$$

where N, Ψ, k, d, θ and β are the number of array elements, progressive phase, wave number, elements' spacing, elevation angle of observation point and progressive phase lead current excitation, respectively.

For an array, different scan angles can be used for different MIMO elements. Recalled from antenna theory, scan angle of θ_0 can be achieved by choosing β as follows [Balanis, 1997], [Allen & Ghavami, 2005]:

$$\beta = -kd\cos\theta_0 \tag{4}$$

3.2 Scattered field calculation

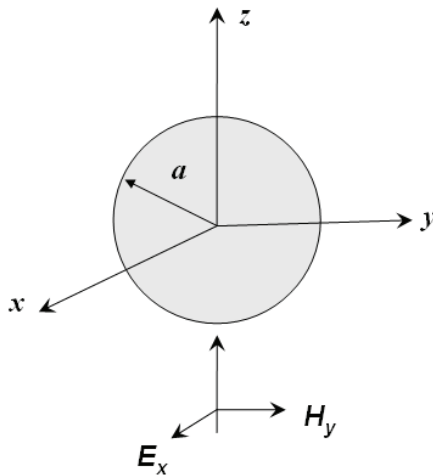Consider a sphere of radius *a* located at the origin as it is shown in Fig. 2.

Fig. 2. A sphere of radius a located at the origin as a scatterer.

Assuming a uniform plane wave polarized in the x direction traveling along the z-axis is incident upon this sphere, the incident electric field is given by:

$$\begin{cases} E_i = E_0 e^{-jkr} \vec{a}_x \\ k = \omega\sqrt{\mu\varepsilon} \end{cases} \tag{5}$$

where E_0 is the incident field amplitude, ω is angular velocity, k, μ and ε are the wave number, electric permeability and permittivity of surrounding medium, respectively. Then the far-field expressions for scattered field from the spherical scatterer at a point (r, θ_i, φ_i) can be written as:

$$\vec{E}^S = E_0 \frac{e^{-jkr}}{r}(E_\theta^S \vec{a}_\theta + E_\varphi^S \vec{a}_\varphi) \tag{6}$$

where E_θ^S and E_φ^S are as follows [Svantesson, 2001]:

$$\begin{cases} \vec{E}_\theta^S = \dfrac{j\cos\varphi_i}{k} \times \sum_{n=1}^{\infty} j^n \dfrac{2n+1}{n(n+1)}[a_n u_1(\theta_i) - b_n u_2(\theta_i)] \\ \vec{E}_\varphi^S = \dfrac{j\sin\varphi_i}{k} \times \sum_{n=1}^{\infty} j^n \dfrac{2n+1}{n(n+1)}[a_n u_2(\theta_i) - b_n u_1(\theta_i)] \end{cases} \tag{7}$$

where $u_1(\theta_i)$ and $u_2(\theta_i)$ are:

$$\begin{cases} u_1(\theta_i) = \sin\theta_i P_n^{1'}(\cos\theta_i) \\ u_2(\theta_i) = \dfrac{P_n^1(\cos\theta_i)}{\sin\theta_i} \end{cases} \tag{8}$$

where, P_n^m is the "Associated Legendre Function" [Balanis, 1989] and assuming that the permeability of the sphere is the same as surrounding environment, a_n and b_n can be written as:

$$\begin{cases} a_n = \dfrac{-k^2 j_n(s)[s_1 j_n(s_1)]' + k_1^2 j_n(s_1)[s j_n(s)]'}{k^2 h_n^{(2)}(s)[s_1 j_n(s_1)]' - k_1^2 j_n(s_1)[s h_n^{(2)}(s)]'} \\[4mm] b_n = \dfrac{-j_n(s)[s_1 j_n(s_1)]' + j_n(s_1)[s j_n(s)]'}{h_n^{(2)}(s)[s_1 j_n(s_1)]' - j_n(s_1)[s h_n^{(2)}(s)]'} \end{cases} \tag{9}$$

where $j_n(x)$ is the "Spherical Bessel Function" of order n, $h^{(2)}{}_n(x)$ is the "Spherical Hankel Function" of the second kind of order n [Balanis, 1989] and a_n, b_n are coefficient dependent on the electrical size of the spherical scatterer and s and s_1 are defined by:

$$\begin{cases} s_1 = k_1 a \\ s = k\ a \end{cases} \tag{10}$$

where k_1, k and a are the wave number for the spherical scatterer, free space wave number and scatterer radius, respectively.

The infinite summation is approximated by taking only a limited number of terms (n_c). A rule of thumb of how many terms that should be evaluated is [Svantesson, 2001]:

$$n_c = s + 4.05 s^{1/3} + 2 \tag{11}$$

Finally in order to have large amount of scattering, electrical conductivity should be chosen high enough. Therefore, the dielectric properties of the conducting scatterers are assumed as follows:

$$\begin{cases} \varepsilon_s = \varepsilon_0 (1 - j100) \\ \mu = \mu_0 \end{cases} \tag{12}$$

where ε_0 and μ_0 are surrounding medium's (air) electrical permittivity and magnetic permeability, respectively.

3.3 Reflected field calculation

To simulate the indoor scenario, transmitter, receiver and the scatterers are located in a simple cubic room, the dimensions of which can be changed. For each single antenna at Tx and Rx in a simple cubic room, six reflecting points exist. For example for a 4×4 MIMO. for the sixteen existing channels, 96 reflection points exist. For each transmitter and receiver set, reflecting points from different walls are found in terms of the dimensions of the wall and the position of Tx and Rx.

To visualize the geometry easier, two reflecting points A_1 and A_5 corresponding to walls1 and 5 and their planes of incidence are shown in Fig. 3.

As it is shown in Fig. 4, two triangles of ABC and AB'C' are similar and hence reflecting point, A, can be obtained as follows:

$$\begin{cases} \dfrac{AB}{AB'} = \dfrac{BC}{B'C'} = \text{Known} \\[3mm] BA + AB' = BB' = \text{Known} \end{cases} \quad \Rightarrow \quad AB \text{ and } AB' \text{ can be obtained} \tag{13}$$
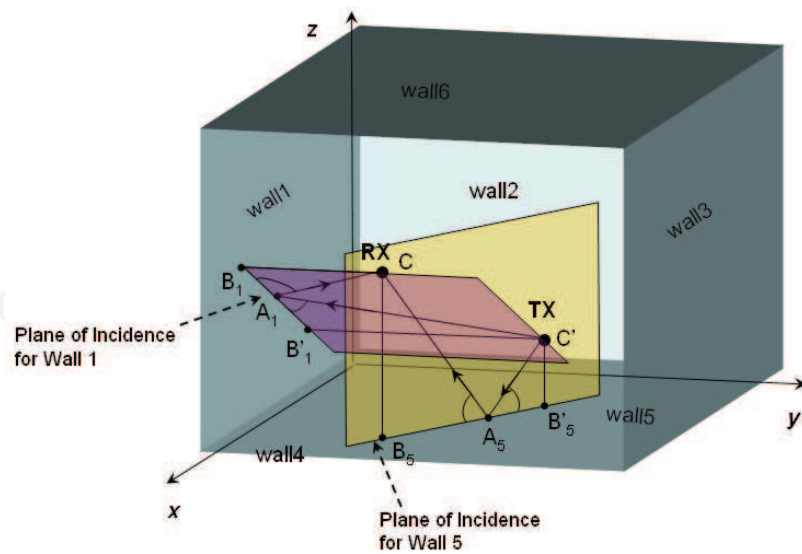
Fig. 3. 3-D geometry of two reflecting points.

where BB′ is the distance between projection points of Rx and Tx on the wall and BC and B′C′ are the distances between Rx and Tx and the wall, respectively.
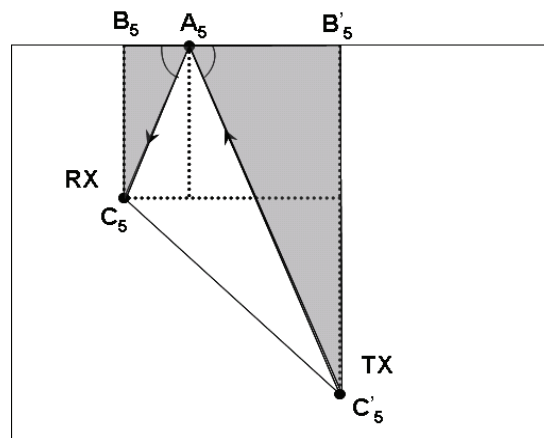

Fig. 4. 2-D Geometry of reflecting points in the plane of incidence.

As an example, A_5, reflecting point of wall5 can be found from two equations given below:

$$\begin{cases} \dfrac{A_5B_5}{A_5B'_5} = \dfrac{B_5C_5}{B'_5\,C'_5} = \dfrac{z_{RX} - z_{wall5}}{z_{TX} - z_{wall5}} \\ B_5A_5 + A_5B'_5 = B_5B'_5 = \sqrt{(x_{RX} - x_{TX})^2 + (y_{RX} - y_{TX})^2} \end{cases} \quad (14)$$

Other reflecting points can also be found in a similar way.

After finding all the reflecting points, the electric fields originated at Tx side and reflected from theses points and terminated at Rx side can be calculated. These fields must be added to those obtained from all scatterers and the direct path between Tx and Rx to get the total electric field. Since the reflection coefficient is different for transverse or perpendicular (Γ_{TE}) and parallel (Γ_{TM}) polarization of electric field relative to the plane of incidence, received electric field on the boundary should be decomposed into Transverse Electric (TE) and Transverse Magnetic (TM) polarizations. Plane of incidence is the plane containing both a normal to the boundary

and the incident wave's propagation direction [Wentworth, 2005]. This plane is shown in Fig. 4.

To decompose electric field components for wall5, for instance, E_x and E_y, each are split into two polarizations of E_x^{TM}, E_x^{TE} and E_y^{TM}, E_y^{TE}, respectively (Fig. 5):

$$\begin{cases} E_x^{TM} = E_x \cos(\psi)\Gamma_{TM} \\ E_x^{TE} = E_x \sin(\psi)\Gamma_{TE} \end{cases} \tag{15}$$

$$\begin{cases} E_y^{TM} = E_y \sin(\psi)\Gamma_{TM} \\ E_y^{TE} = E_y \cos(\psi)\Gamma_{TE} \end{cases} \tag{16}$$

where $\psi = \arctan\dfrac{y_{cross}}{x_{cross}}$ and Γ_{TE} and Γ_{TM} are reflection coefficients of TE and TM polarizations, respectively and are shown in Fig. 5.
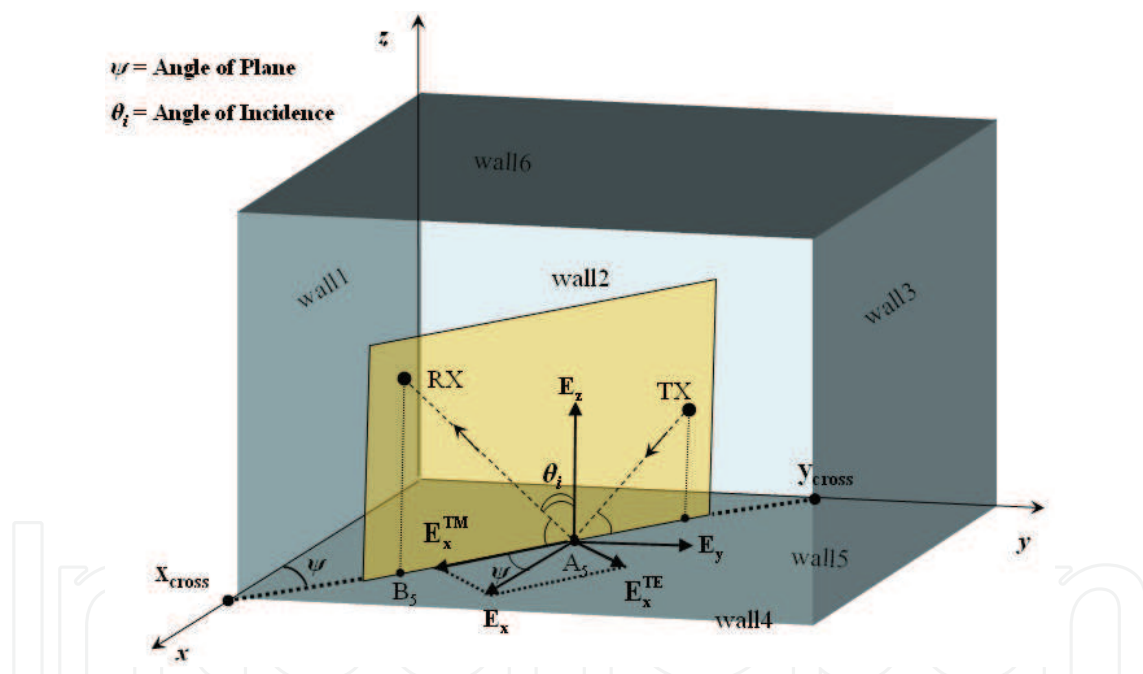

Fig. 5. 3-D view of electric field decomposition to TM and TE polarizations at the reflecting point.

Since E_z itself is the parallel component (TM), it does not need to be decomposed and hence to find its corresponding reflected field, it should be simply multiplied by Γ_{TM}.

After finding TM and TE components of reflected waves, they should be converted to previous global coordinates for further process:

$$\begin{cases} E_x' = E_x^{TM} \cos(\psi) + E_x^{TE} \sin(\psi) \\ E_y' = E_y^{TM} \sin(\psi) + E_y^{TE} \cos(\psi) \end{cases} \tag{17}$$

where $E_x^{'}$ and $E_y^{'}$ are the x and y components of the reflected electric field from wall5. The same procedure is applicable for other walls. To find Γ_{TM} and Γ_{TE}, angles of incidence and transmission are required [Wentworth, 2005]:

$$\begin{cases} \Gamma_{TE} = \dfrac{\eta_2 \cos(\theta_i) - \eta_1 \cos(\theta_t)}{\eta_2 \cos(\theta_i) + \eta_1 \cos(\theta_t)} \\[2ex] \Gamma_{TM} = \dfrac{\eta_2 \cos(\theta_t) - \eta_1 \cos(\theta_i)}{\eta_2 \cos(\theta_t) + \eta_1 \cos(\theta_i)} \end{cases} \qquad (18)$$

where (η_1, η_2), (θ_i, θ_t) are the intrinsic impedances of free space and wall material and angles of incidence and transmission, respectively. Referring to Fig. 5, one can easily calculate angles of incidence and transmission for wall5 as follows:

$$\begin{cases} \theta_i = \dfrac{\pi}{2} - \arctan \dfrac{h_{Rx}}{B_5 A_5} \\[2ex] \theta_t = \arcsin \dfrac{k_1 \sin(\theta_i)}{k_2} \end{cases} \qquad (19)$$

where (θ_i, θ_t), h_{Rx}, (k_1, k_2) are angles of incidence and transmission, Rx height and wave number of air and wall material, respectively.

3.4 Channel capacity calculation

Assuming that the channel is unknown to the transmitter and the total transmitted power is equally allocated to all N_T antennas, the capacity of the system is given by [Foschini & Gans, 1998]:

$$C = \log_2 \left(\left(\det\left[\mathbf{I_{N_T}} + \frac{SNR}{N_T} \times \frac{\mathbf{HH^*}}{\text{norm}(HH^*)} \right] \right) \right) \quad \text{bps/Hz} \qquad (20)$$

where $\mathbf{I_{N_T}}$ is the identity matrix, SNR is the average signal to noise ratio within the receiver aperture, N_T is the number of transmitter antennas, $\mathbf{H}$ is the $N_T \times N_R$ channel matrix and $\mathbf{H^*}$ is the conjugate transpose of $\mathbf{H}$. To calculate $\mathbf{H}$-matrix baseband channel complex impulse response should be computed for scatterers, reflectors and direct path corresponding to each channel.

1. Scatterers

$$h_{scatterers} = \sum_{q=1}^{N_S} \frac{e^{-jk(|\vec{r}_{msq}| + |\vec{r}_{sqb}|)}}{(|\vec{r}_{msq}| \times |\vec{r}_{sqb}|)} [E_\theta(\vec{r}_{bs}) \cdot \vec{\ell}_{eff\theta} + E_\varphi(\vec{r}_{bs}) \cdot \vec{\ell}_{eff\varphi}] \qquad (21)$$

where $N_S, \vec{r}_{msq}, \vec{r}_{sqb}, (E_\theta, E_\varphi), (\vec{\ell}_{eff\theta}, \vec{\ell}_{eff\varphi})$ are the number of scatterers, distance vector from Tx (MS) to q^{th} scatterer, distance vector from Rx (BS) to q^{th} scatterer, effective radiation pattern at Rx in $\vec{a}_\theta$ and $\vec{a}_\varphi$ directions (radiation patterns of Tx and Rx are included in effective radiation pattern), and effective lengths of the half-wavelength dipole in $\vec{a}_\theta$ and $\vec{a}_\varphi$ directions, respectively.

Assuming that the half-wavelength dipole antenna is connected to a matched load and current distribution is sinusoidal, two components of effective complex length of dipole can be obtained from [Collin, 1985]:

$$\begin{cases} \vec{\ell}\text{eff}_\theta = \dfrac{\lambda}{\pi} \dfrac{E_\theta}{|E_0|} \\[3mm] \vec{\ell}\text{eff}_\varphi = \dfrac{\lambda}{\pi} \dfrac{E_\varphi}{|E_0|} \end{cases} \tag{22}$$

where E_θ and E_ϕ are the electric fields radiated by the half-wavelength dipole while it is in transmitting mode.

2.   Reflectors

$$h_{\text{reflectors}} = \sum_{q=1}^{N_r} \frac{e^{-jk(|\vec{r}_{mrq}|+|\vec{r}_{rqb}|)}}{(|\vec{r}_{mrq}| \times |\vec{r}_{rqb}|)} [E_\theta(\vec{r}_{br}) \cdot \vec{\ell}_{\text{eff}\theta} + E_\varphi(\vec{r}_{br}) \cdot \vec{\ell}_{\text{eff}\varphi}] \tag{23}$$

where $N_r, \vec{r}_{mrq}, \vec{r}_{rqb}, (E_\theta, E_\varphi), (\vec{\ell}_{\text{eff}\theta}, \vec{\ell}_{\text{eff}\varphi})$ are the number of reflectors, distance vector from Tx to q^{th} reflector (wall), distance vector from Rx to q^{th} reflector, effective radiation pattern at Rx in $\vec{a}_\theta$ and $\vec{a}_\varphi$ directions, and effective lengths of the half-wavelength dipole in $\vec{a}_\theta$ and $\vec{a}_\varphi$ directions, respectively.

3.   Direct Path

To obtain direct field between Tx and Rx, the following equation is used:

$$h_{\text{direct}} = \frac{e^{-jk|\vec{r}_{mb}|}}{|\vec{r}_{mb}|} [E_\theta(\vec{r}_{bm}) \cdot \vec{\ell}_{\text{eff}\theta} + E_j(\vec{r}_{bm}) \cdot \vec{\ell}_{\text{eff}\varphi}] \tag{24}$$

where $\vec{r}_{mb}, (E_\theta, E_\phi), (\vec{\ell}_{\text{eff}\theta}, \vec{\ell}_{\text{eff}\phi})$ are the distance vector from Tx to Rx, effective radiation pattern at Rx in $\vec{a}_\theta$ and $\vec{a}_\varphi$ directions and the effective lengths of the half-wavelength dipole in $\vec{a}_\theta$ and $\vec{a}_\varphi$ directions, respectively.

3.5 Coordinate transformations

To find the total electric field at Rx which is the last destination of the traveled wave, many coordinate transformations should be performed. Since, it is much easier to transform rectangular coordinates of local and global systems rather than spherical ones, before each transformation step, electric field in rectangular coordinate should be found.

Equation (25) is used frequently while developing the mathematical model. It is a general formula to rotate a coordinate system and convert it to the other one by knowing the angles between their axes.

$$\underbrace{\begin{bmatrix} \hat{u}_1 \\ \hat{u}_2 \\ \hat{u}_3 \end{bmatrix}}_{New\_System} = \underbrace{\begin{bmatrix} \hat{a}_1 \cdot \hat{u}_1 & \hat{a}_2 \cdot \hat{u}_1 & \hat{a}_3 \cdot \hat{u}_1 \\ \hat{a}_1 \cdot \hat{u}_2 & \hat{a}_2 \cdot \hat{u}_2 & \hat{a}_3 \cdot \hat{u}_2 \\ \hat{a}_1 \cdot \hat{u}_3 & \hat{a}_2 \cdot \hat{u}_3 & \hat{a}_3 \cdot \hat{u}_3 \end{bmatrix}}_{Rotation\_Matrix} \underbrace{\begin{bmatrix} \hat{a}_1 \\ \hat{a}_2 \\ \hat{a}_3 \end{bmatrix}}_{Old\_System} \tag{25}$$

The given solution in (7) is for an x oriented field propagation along the z-axis. However, these conditions will rarely be met since the same coordinate system is used for all scatterers. By employing a local coordinate system for each object, the mentioned solution can be applied.

Different local and global coordinates are shown in Fig. 6 and defined as follows:

- Gmain (x_{Gmain}, y_{Gmain}, z_{Gmain}) is the global coordinate.
- G1 (x_{G1}, y_{G1}, z_{G1}) is a parallel coordinate system with Gmain and its origin is on the center of Tx.
- L1 (x_{L1}, y_{L1}, z_{L1}) is the local coordinate for Tx antenna and its origin is the same as that of G1 and also for this coordinate system z_{L1} is chosen along the direction of Tx dipole and x_{L1} is defined on the plane of x_{G1} and y_{G1}.
- L2 (x_{L2}, y_{L2}, z_{L2}) is the local coordinate for scatterers and its origin is on the scatterer center and for this coordinate system z_{L2} is chosen along the direction of r_{L1} and x_{L2} is chosen along the direction of $\hat{\theta}_{L1}$. r_{L1}, θ_{L1}, φ_{L1} are spherical coordinate components of each scatterer in respect to *L1* coordinate. It is worth mentioning that for each scatterer an *L2* coordinate is defined.
- *L3* (x_{L3}, y_{L3}, z_{L3}) is the local coordinate for Rx antenna the origin of which is on the center of Rx and also for this coordinate system z_{L3} is chosen along the direction of Rx dipole and x_{L3} is defined on a plane parallel to the plane of x_{Gmain} and y_{Gmain}.
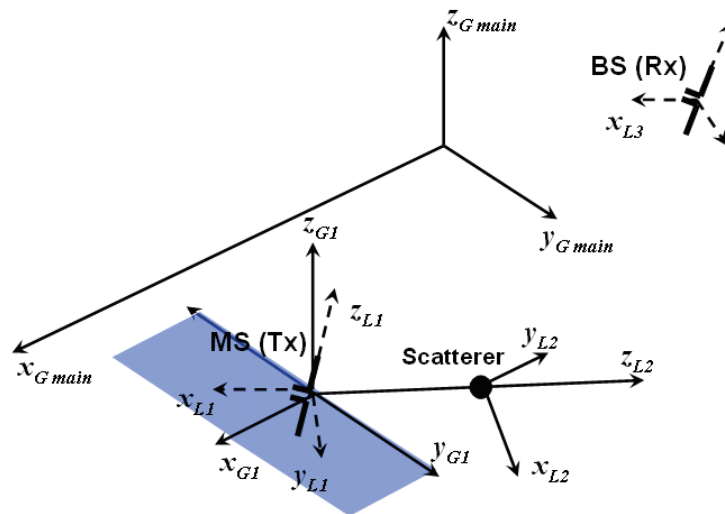

Fig. 6. Global and local coordinates and dipole antennas at both ends.

The local coordinates L1 and L3 are defined to provide the possibility of using different polarizations for Tx and Rx antennas, respectively.

Now to fulfill the condition required for using the scattering formulas, L1 coordinate system should be converted to L2 coordinate system which is the local coordinate system of each scatterer. If the scatterer is located at (r_{L1}, θ_{L1}, φ_{L1}) in respect to L1 coordinate system, to convert L1 into L2 coordinates system, one can use:

$$\begin{bmatrix} \hat{x} & \hat{y} & \hat{z} \end{bmatrix}_{L2} = \begin{bmatrix} \hat{x} & \hat{y} & \hat{z} \end{bmatrix}_{L1} \begin{bmatrix} \cos\theta_{L1}\cos\varphi_{L1} & -\sin\varphi_{L1} & \sin\theta_{L1}\cos\varphi_{L1} \\ \cos\theta_{L1}\sin\varphi_{L1} & \cos\varphi_{L1} & \sin\theta_{L1}\sin\varphi_{L1} \\ -\sin\theta_{L1} & 0 & \cos\theta_{L1} \end{bmatrix} \qquad (26)$$

where θ_{L1} and φ_{L1} are scatterer's coordinates referring to L1.

If the Tx antenna type is something other than dipole or generally, is an antenna with electric field in both $\hat{\theta}$ and $\hat{\varphi}$ directions then the relation between the L1 and L2 coordinate systems is more complicated and the corresponding rotation matrix is as follows:

$$[\hat{x} \ \hat{y} \ \hat{z}]_{L2} = [\hat{x} \ \hat{y} \ \hat{z}]_{L1} \times \frac{1}{A} \times$$

$$\begin{bmatrix} E_\theta \cos\theta_{L1}\cos\varphi_{L1} - E_\varphi \sin\varphi_{L1} & -E_\varphi \cos\theta_{L1}\cos\varphi_{L1} - E_\theta \sin\varphi_{L1} & A\sin\theta_{L1}\cos\varphi_{L1} \\ E_\theta \cos\theta_{L1}\sin\varphi_{L1} + E_\varphi \cos\varphi_{L1} & -E_\varphi \cos\theta_{L1}\sin\varphi_{L1} + E_\theta \cos\varphi_{L1} & A\sin\theta_{L1}\sin\varphi_{L1} \\ -E_\theta \sin\theta_{L1} & +E_\varphi \sin\theta_{L1} & A\cos\theta_{L1} \end{bmatrix} \quad (27)$$

where E_θ, E_φ are the electric field components at each scatterer center referred to L1 and θ_{L1} and φ_{L1} are scatterer's coordinates and $A=\sqrt{E_\theta^2 + E_\varphi^2}$. Equation (27) is simplified to rotation matrix in (26) if Tx antennas has electric field only in θ direction.

Finally, after all conversions of coordinate systems, the vectors which are necessary to find channel complex impulse response such as electric fields and effective lengths should be converted to the main global coordinate which is specified as G_{main} in Fig. 6.

4. Verifying the SISTER model

To verify the obtained results from developed model, "Wireless Insite" software by Remcom Inc. [Remcom Inc., 2004] is used. This software is a three-dimensional ray tracing tool for both indoor and outdoor applications which models the effects of surrounding objects on the propagation of electromagnetic waves between Tx and Rx.

In order to accomplish this verification, different steps have been taken. First, only a direct path between Tx and Rx is considered for a Single Input Single Output (SISO) system and received power is verified by both Friis equation and ray tracing tool.

It is assumed that a half wavelength dipole antenna (Gain=2.16dBi) is used at both ends, Tx-Rx distance is 2.7m, both Tx and Rx heights are 1.5m and transmitted power is 0dBm (1mW). For the mentioned system configuration, numerical results obtained from both proposed mathematical model and ray tracing are summarized in Table 1.

	$P_{received}$	$|E_z|$ (V/m)	Phase E_z (degree)
SISTER Model	-44.362 dBm (3.663×10^{-8} W)	0.117	76.917
Ray Tracing	-44.350 dBm (3.673×10^{-8} W)	0.117	73.496
Friis Equation	-44.337dBm (3.684×10^{-8} W)	-------	-------

Table 1. Numerical results for a SISO system.

As it can be seen the result obtained from the SISTER model matches well with a fractional error less than 0.006 with both ray tracing tool and also Friis transmission equation given in (28) [Balanis, 1997]:

$$\frac{P_r}{P_t} = (\frac{\lambda}{4\pi R})^2 G_r G_t \tag{28}$$

where P_r, P_t, λ, R, G_r and G_t are received power, transmitted power, wavelength, Tx-Rx distance and Rx and Tx antenna gains, respectively.

In the next step (Fig. 7) one wall is added to the previous system configuration and the reflected ray is evaluated as well. For this case, summarized results can be found in Table 2 which again shows an acceptable match with those of the ray tracing. The same procedure to validate the reflected field has been done for all six walls and all have shown good match.
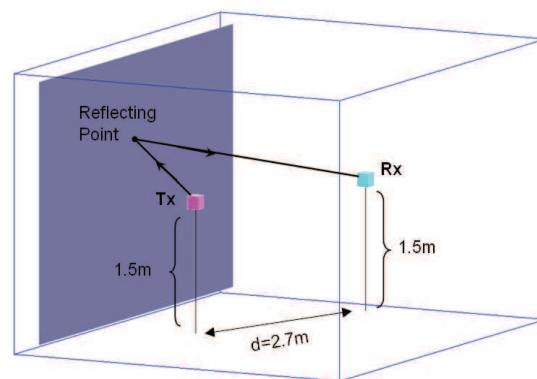
Fig. 7. Ray tracing visualization of a SISO system in an indoor environment considering reflection from one wall.

	$P_{received}$	$|E_z|$ (V/m)	Phase E_z (degree)
SISTER Model	-48.442 dBm (1.432×10^{-8} W)	0.073	-115.719
Ray Tracing	-48.461 dBm (1.425×10^{-8} W)	0.073	-121.210

Table 2. Numerical results for a SISO system configuration shown in Fig. 7

Channel capacity for the MIMO system configuration illustrated in Fig. 8 is compared for both proposed model and ray tracing tool. Fig. 9 shows the results for three cases; direct path only, reflected paths only, total paths.
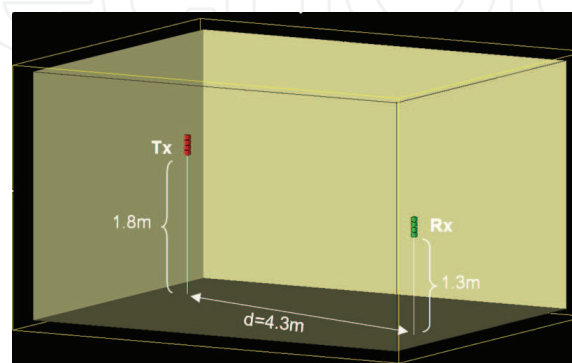

Fig. 8. Ray tracing visualization of a 4×4-MIMO system in an indoor environment considering six walls.

As the final step to verify the results, the capacity of MIMO systems with different $N_T \times N_R$ antenna numbers are evaluated in an outdoor environment for NLOS case and the results are compared with Rayleigh model for similar antenna numbers. Fig. 10 shows the capacities obtained from simulated Rayleigh channel by MATLAB and SISTER model applied to an outdoor NLOS environment with 30 scatterers for different numbers of antennas.

As these results show good agreement with both ray tracing tool and Rayleigh model is achieved.
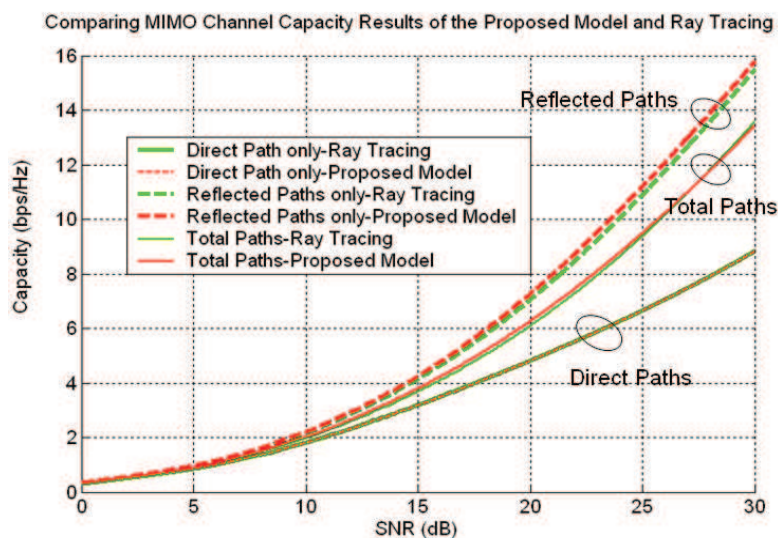

Fig. 9. Comparing MIMO channel capacity obtained from SISTER model and ray tracing tool for different rays.
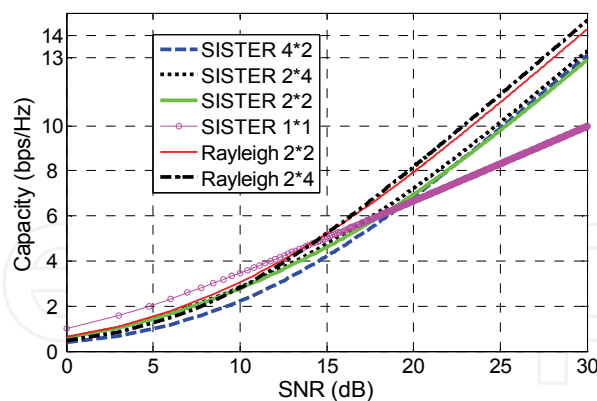

Fig. 10. Comparing channel capacity obtained from SISTER model and Rayleigh model.

The MIMO configuration is the same as Fig.8 and the room dimensions are 5×4×3 m³ and a wall exists to block the LOS path.

5. Results of applying SISTER model for different scenaris

Although the SISTER model is sufficiently general to be applied to any distributions and locations for the scatterers, here we concentrate only on picocell environments.

Moreover, "Angle Diversity" which is a new promising solution and has recently attracted considerable attention in MIMO system designs [Allen et al., 2004] is also evaluated model and compared with well-known "Space Diversity" method by applying the SISTER. In this method, instead of multiple antennas used in space diversity case, multiple simultaneous beams are assumed at both sides. The main advantage of this technique comparing is that it allocates high capacity not to all the points in space, but the desired ones. This results in minimum undesired interference. The main difficulty in such systems, however, is the beam cusps (beam overlaps) [Allen & Beach, 2004] and finding the optimal angles where the different beams should be directed towards. We have investigated the use of antenna array in angle diversity case to implement the narrow beams needed in this method. We also have addressed some problems with beam cusps which introduce correlations in MIMO channels, and suggested some solutions to overcome this problem.

Here, various results are presented which are ultimately useful to set the system design parameters and to evaluate and compare the performance of MIMO systems using space or angle diversity for both outdoor and indoor environments. Due to space limitations only some of the results are presented here and more results can be found in [E.Forooshani, 2006].

5.1 SISTER results for outdoor environments

Outdoor system specifications considered are summarized in Table 3. Tx refers to transmitter and Rx refers to receiver antennas. Without loosing the generality, it is assumed that mobile set (MS) is the transmitter and the base station (BS) is the receiver side. All simulations are done based on working frequency of 2.4GHz. For results shown in Figs 11-15, a 4×4 MIMO system is considered.

Two common scatterer distributions for outdoor environments are uniform distribution around each end and cluster distribution, as shown in Fig. 11(a) and Fig. 11(b), respectively.

	Tx (MS) height	Rx (BS) height	Relative height of Tx and Rx	Distance between Tx and Rx
Outdoor System	24λ (3m)	40λ (5m)	16λ (2m)	102λ (13m)

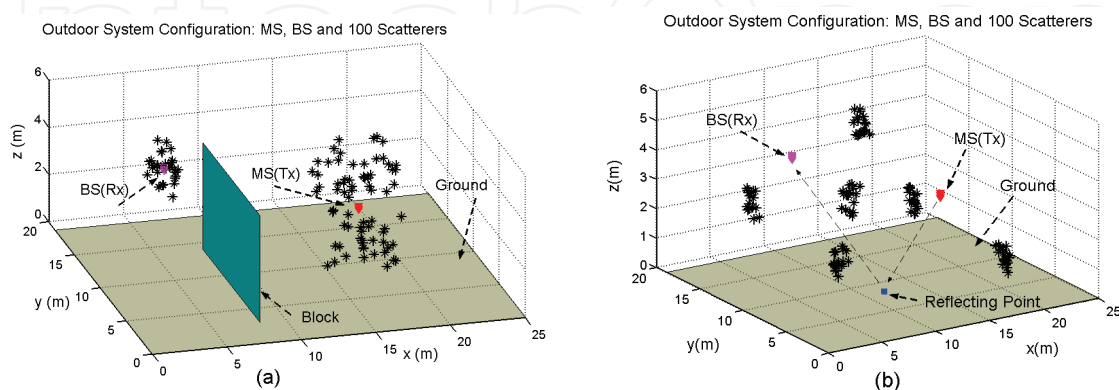Table 3. Outdoor system specifications.

Fig. 11. Outdoor system configuration for: (a) NLOS scenario with uniformly distributed scatterers around both ends, (b) LOS scenario with cluster form scatterers in a cubic volume ($200\lambda \times 150\lambda \times 50\lambda$ or $25 \times 18.75 \times 6.25$, m^3).

5.1.1 Impact of ground material

For outdoor environment, impact of two types of ground material, high and low conductive ones (Fig. 12) are investigated. Reflection from the high conductive ground contributes as much as the direct path and its presence can suppress the effect of direct path and hence increase the capacity comparing to the low conductive ground case. It also shows that for a ground with conductivity more than 100 S/m, capacity is mainly controlled by the reflected path from the ground and scatterers do not contribute much in the channel capacity.
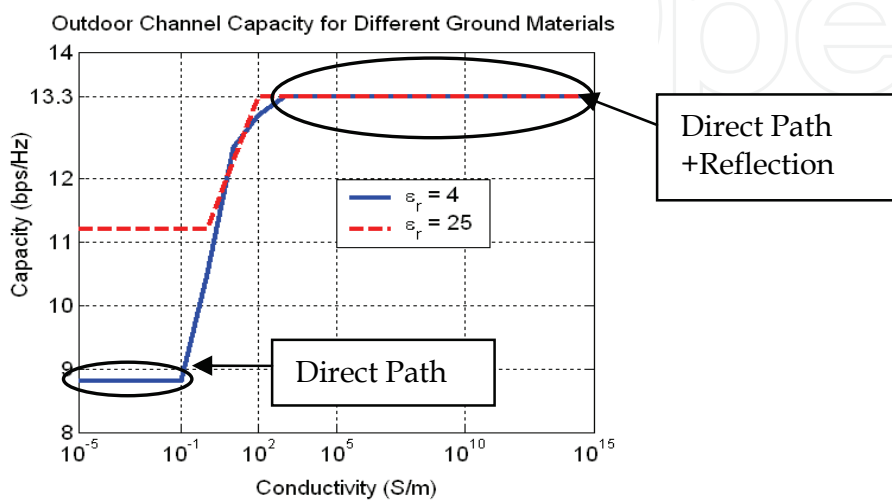

Fig. 12. Channel capacity at signal to noise ratio, SNR=30dB for different ground materials (ε_r=4, ε_r=25) considering 30 uniformly distributed scatterers, the LOS case.

5.1.2 Impact of number of scatterers

Figs. 13 and 14 show the impact of number of uniformly distributed scatterers in terms of channel capacity versus SNR. Typical number of scatterers for this study is 30. In NLOS case, it is assumed that there is no direct path but reflection from the ground exists (blocked LOS or quasi-LOS). Fig. 13 shows the LOS case. In this case reflection from the high conductive ground contributes as much as the direct path. Therefore, its presence can suppress the effect of direct path and hence increase the capacity in compare to the low conductive ground case.

For NLOS case, shown in Fig. 14, when the number of scatterer is not high (30 scatterers) reflection from the high conductive ground creates the dominant path and capacity is low. When the number of scatterers is high enough (100 scatterers), they are able to lessen the effect of reflection from the ground and in this case capacity is higher. For low conductive ground, on the other hand, the reflection from the ground is so weak that no dominant path exists and hence for both cases of 30 and 100 scatterers, channel capacity is high.

5.1.3 Comparing space and angle diversities

To compare space and angle diversity methods for a 4×4-MIMO system, a scenario consisting of four clusters of scatterers is considered. The length occupied by antenna elements is the same for both space and angle diversity methods. It is essential to keep the array length the same if we intend to have a fair comparison between the two methods in terms of system size and length. Antenna array length at both ends is 1.5λ.

For space diversity case, four antenna elements are used while in angle diversity the same four elements are used along with a Butler matrix to create four simultaneous beams with different scan angles. Assumptions made for space and angle diversity methods are summarized in Table 4.
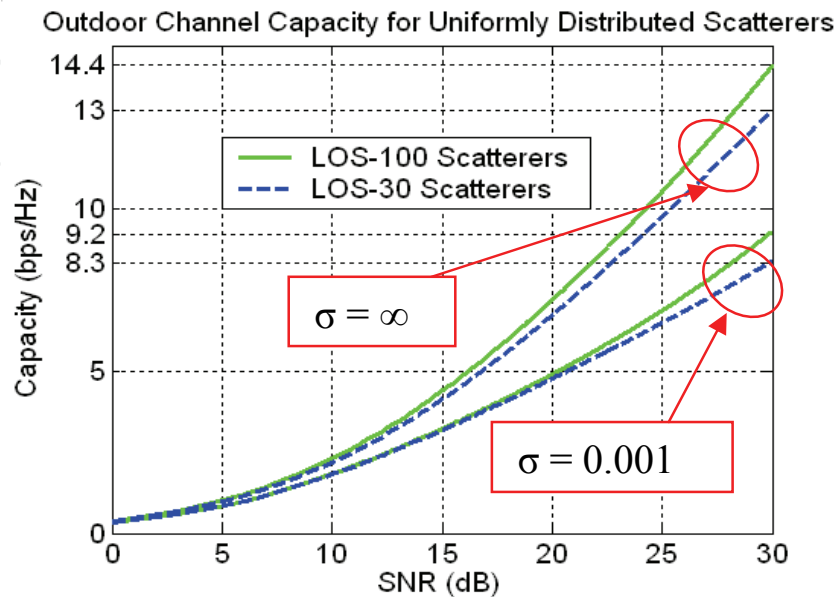

Fig. 13. Channel capacity for different number of scatterers distributed uniformly around both ends in LOS case (σ=ground's electrical conductivity, S/m).
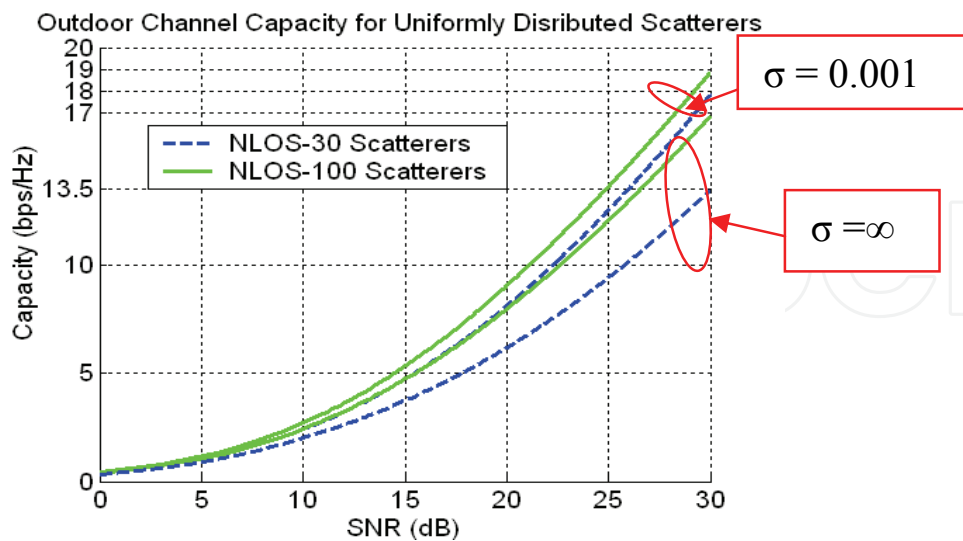

Fig. 14. Channel capacity for different numbers of scatterers distributed uniformly around both ends in NLOS case including reflection from the ground but not the direct path (σ=ground's electrical conductivity).

	Number of elements at BS	Number of elements at MS	BS element spacing (*d*-Rx)	MS element spacing (*d*-Tx)
Space Diversity	4	4	0.5λ	0.5λ
Angle Diversity	4	4	0.5λ	0.5λ

Table 4. Assumptions for space and angle diversity methods.

For space and angle diversities channel capacity is calculated based on equations (29) and (30), respectively.

$$C(SNR)=\log_2\left(\det\left[\mathbf{I_{N_T}}+\frac{SNR}{N_T}\times\frac{\mathbf{HH}^*}{norm(\mathbf{HH}^*)}\right]\right) \qquad (29)$$

$$C(SNR)=\log_2\left(\det\left[\mathbf{I_{N_T}}+(G_{Tx}\times G_{Rx})\frac{SNR}{N_T}\times\frac{\mathbf{HH}^*}{norm(\mathbf{HH}^*)}\right]\right) \qquad (30)$$

where C is the channel capacity, $\mathbf{I_{N_T}}$ is the Identity matrix, SNR is the signal to noise ratio, N_T is number of transmitter antennas (or beams) and $\mathbf{H}$ is the channel matrix, whose elements are calculated using the SISTER model. For space diversity h_{ij} is the path gain between antenna element i at BS and j at MS. For angle diversity each h_{ij} represents the path gain between ith beam at BS and jth beam at MS.

Factor ($G_{Tx} \times G_{Rx}$) in (30) shows the array gain of angle diversity method. When an array consists of elements with the spacing of 0.5λ, then its gain is equal to the number of elements if antenna losses are ignored ($G_{Tx} \times G_{Rx}$ =4×4=16). Since it is assumed that the total power is the same for two systems, it is required to take the array gain into account while comparing capacities of two methods in terms of SNR. Note that no mutual coupling effect is assumed in this calculation.

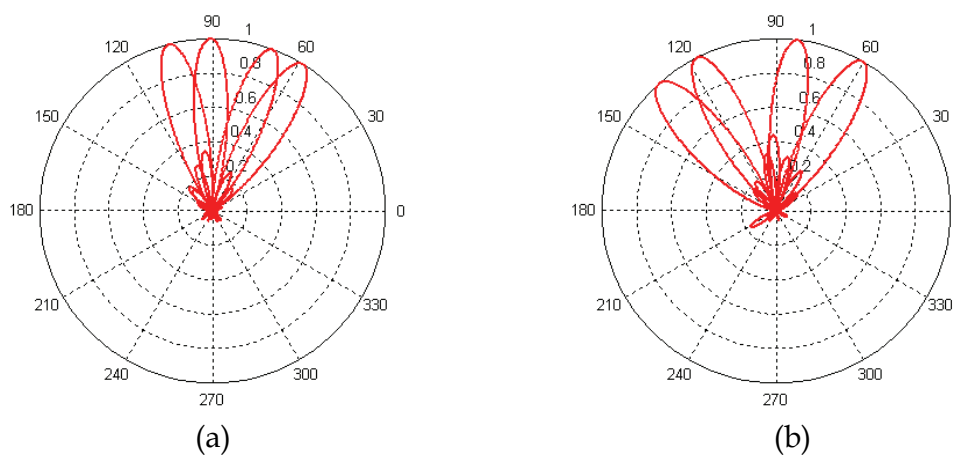Fig.15 shows four beams angels at MS and BS sides for angle diversity case.

(a)   (b)

Fig. 15. Four multibeams which are pointed towards four clusters located in different θ angles (a) MS (Tx) (N-array=4, beam angles=62º, 70º, 91º, 105º), (b) BS (Rx) (N-array=4, beam angles=60º, 83º, 117º, 132º).

Table 5 and Fig. 18 (a) show singular values of normalized **H**-matrix and capacity results for both methods in LOS case, respectively. Table 6 and Fig. 16 (b) show singular values of normalized **H**-matrix and capacity results for both methods in NLOS case, respectively.

As Fig. 16 show angle diversity surpass space diversity significantly, mostly due to the array gain. Even though angle diversity often shows better channel orthogonality, improperly chosen angles caused not to achieve the maximum available capacity for the angle diversity.

	Singular Value1	Singular Value2	Singular Value3	Singular Value4
Space Div.	1.0000	0.0016	0.0004	0.0000
Angle Div.	1.0000	0.0024	0.0008	0.0000

Table 5. Singular values for 30 scatterers in 4 clusters for LOS.

	Singular Value1	Singular Value2	Singular Value3	Singular Value4
Space Div.	1.0000	0.4424	0.0062	0.0003
Angle Div.	1.0000	0.4481	0.0007	0.0000

Table 6. Singular values for 30 scatterers in 4 clusters for NLOS.

For NLOS case, the rays from Tx towards clusters behind the block are stopped which cause reduction in the number of channels. Another reason which has caused getting undesirable results for angle diversity method in both LOS and NLOS cases is the beam cusps. Considering above discussion, for the given scenario, angle diversity seems to be an appropriate alternative for space diversity which can provide similar orthogonality with less interference.
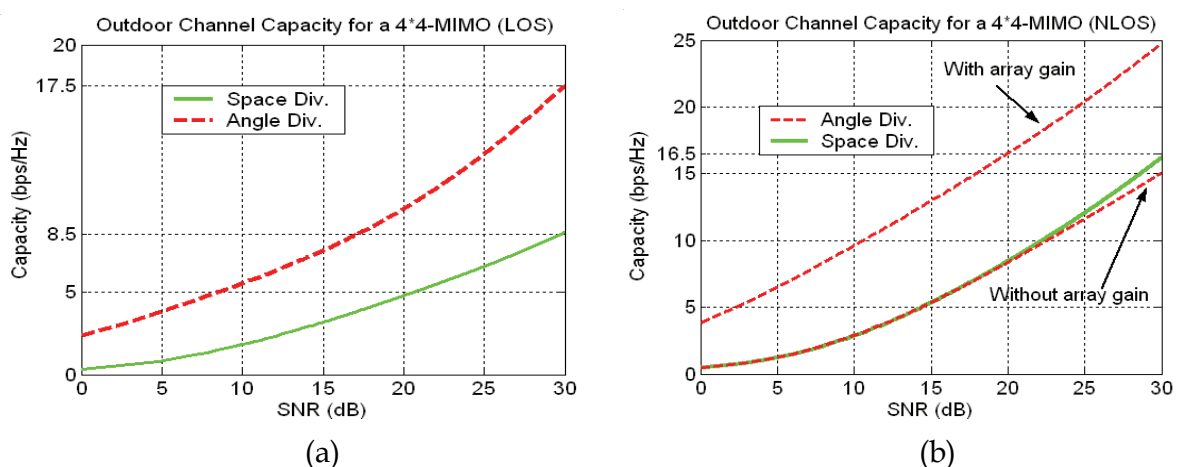

(a) (b)

Fig. 16. Channel capacity for 30 scatterers in 4 clusters for (a) LOS, (b) NLOS.

5.1.4 Impact of number of clusters

The impact of the number of clusters on the channel capacity for a NLOS scenario, similar to what was shown in Fig. 11(b) is also studied. To consider the effects of number of clusters, clusters in this configuration are located in such a way to avoid blockage by the defined obstacle in the middle of the study area. Fig. 17 shows that for a certain amount of SNR, as

the number of clusters increases, at first, channel capacity increases but after a while it remains constant. This is expected as by increasing the number of clusters multipath components are increased and correlation between channels is decreased. However, after a certain point the slope of capacity increase decreases because as the space is limited the clusters are going to be closer to each other and after a while they will have overlaps. This reduces the orthogonality of the channels. These results are also in agreement with those cited in [Burr, 2003] based on "finite scatterer channel model" Also note that as the number of scatters increases and the spacing between them decreases due to the increase in mutual interactions a single interaction models such as SISTER is not accurate anymore.
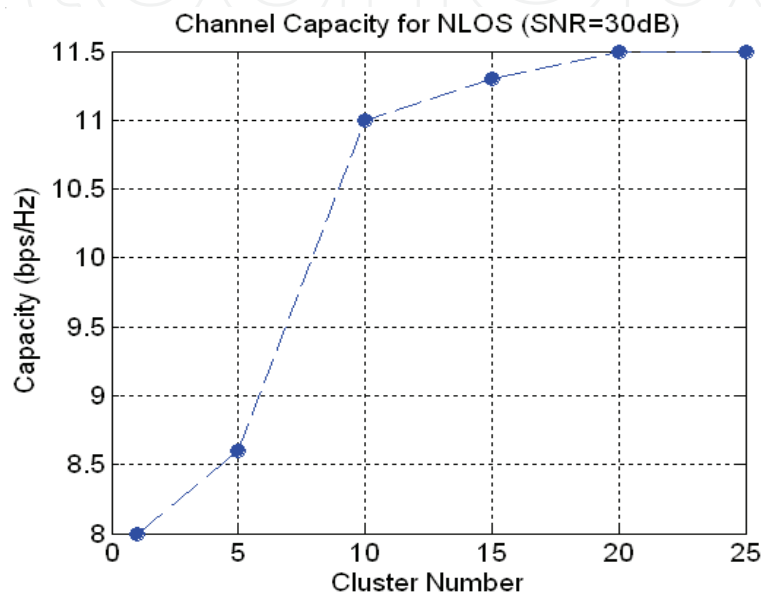

Fig. 17. Channel capacity at SNR=30 dB for different numbers of clusters which contain 10 scatterers each.

5.2 SISTER results for indoor environments
5.2.1 Office area
In order to characterize the indoor channel, the outdoor model is enhanced in such a way that it includes not only the scatterers and reflection from the ground but also reflection from the walls for a typical office area of 5×4×3 m³. Indoor system specifications considered in this study are summarized in Table 7.

	Tx height	Rx height	Relative height of Tx and Rx	Distance between Tx and Rx	Room's dimension	Scatterers' radius	Scatterers' number
Office	10.4λ (1.3m)	14.4λ (1.8m)	4λ (0.5m)	32.24λ (4.3m)	5×4×3(m³)	0.1m	30

Table 7. A typical office area specifications.

Two distributions of uniform and cluster form for scatterers are considered to study an office area (Fig. 18).
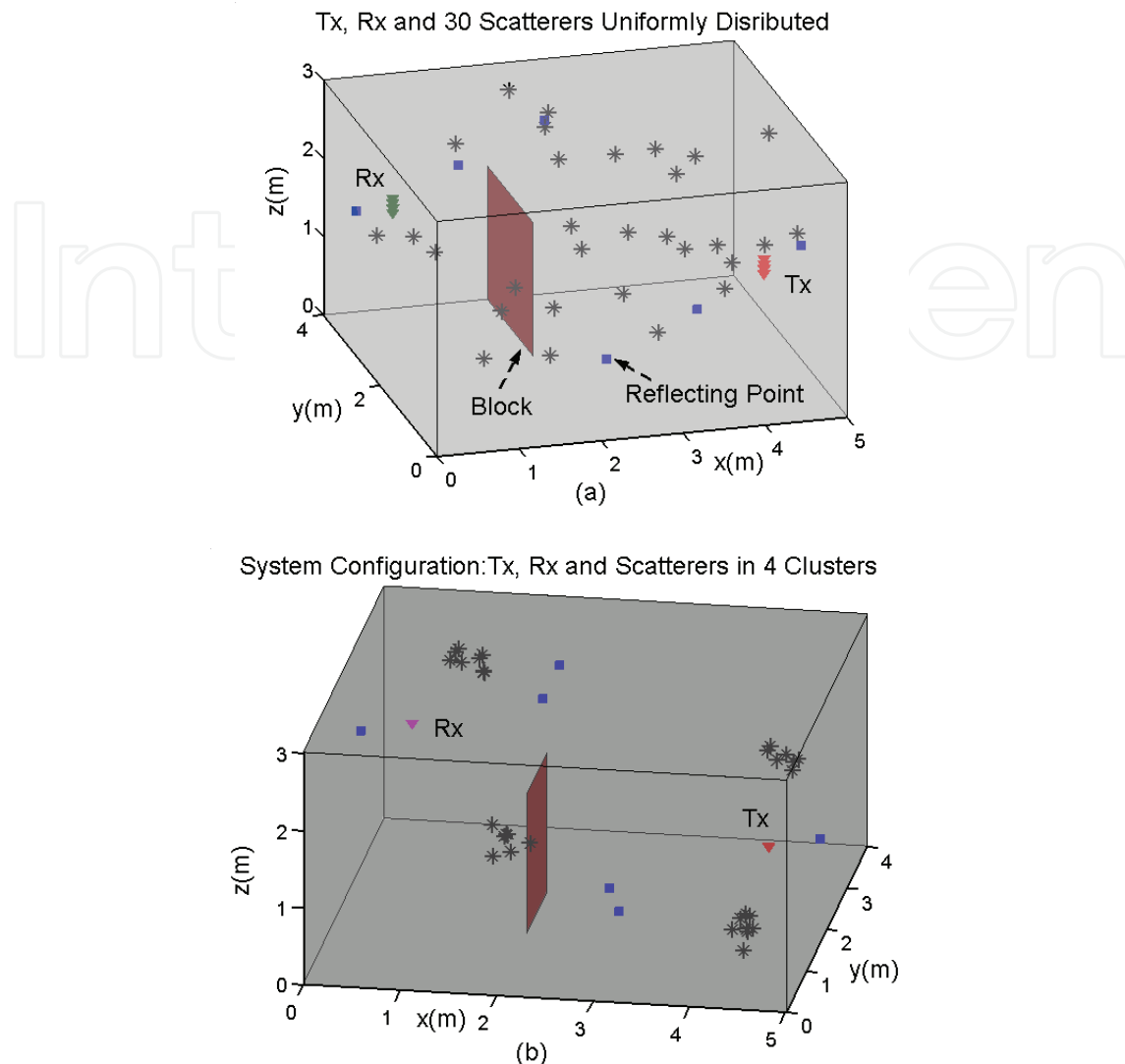
Fig. 18. An office area including Tx, Rx and 30 scatterers distributed (a) uniformly and (b) in cluster form.

5.2.2 Comparing space and angle diversities

Space and angle diversities are compared for different scenarios in [E.Forooshani, 2006] but only results for 30 uniformly distributed and cluster scatterers in indoor are presented here. Selected antenna beams in 2×2-MIMO angle diversity were (62o, 121o) for Tx and (72o, 119o) for Rx. In 4×4-MIMO systems beams were selected at (48o, 65o, 130o, 138o) for both sides. Capacities of both systems are shown in Fig. 19.

The composition of singular values is also given in Table 8. The results show that for the 4×4-MIMO system for both LOS and NLOS cases, angle diversity surpasses space diversity method in terms of channel orthogonality. Moreover, it offers array gain which leads in an increase in the capacity shown in Fig. 19(b). Based on these results, for this system, it is more convenient to apply angle diversity method since LOS and NLOS capacities are similar if the beams are selected properly while this is not true for space diversity. Furthermore, applying angle diversity helps to lessen the interference effects (compare to omnidirectional antennas,

the power is directed to limited angles) in an indoor environment which is a real concern nowadays.

By try and error, it was found that, particularly for LOS case, higher capacity can be achieved by choosing angles far away from the direct path which in most cases is approximately around horizontal plane (θ=90º).

In the 2×2-MIMO for space diversity, instead of 4 elements, there are 2 elements at each end with the spacing of $3\lambda/2$ and for angle diversity; there are two arrays with λ spacing between array centers. Each array consists of 2 dipoles with $\lambda/2$ spacing.

To study angle diversity method for this 2×2-MIMO system in LOS case where 30 scatterers are uniformly distributed, two beams are directed towards the reflecting points of ceiling and the floor which actually are the two angles far from the direct path. For NLOS case,
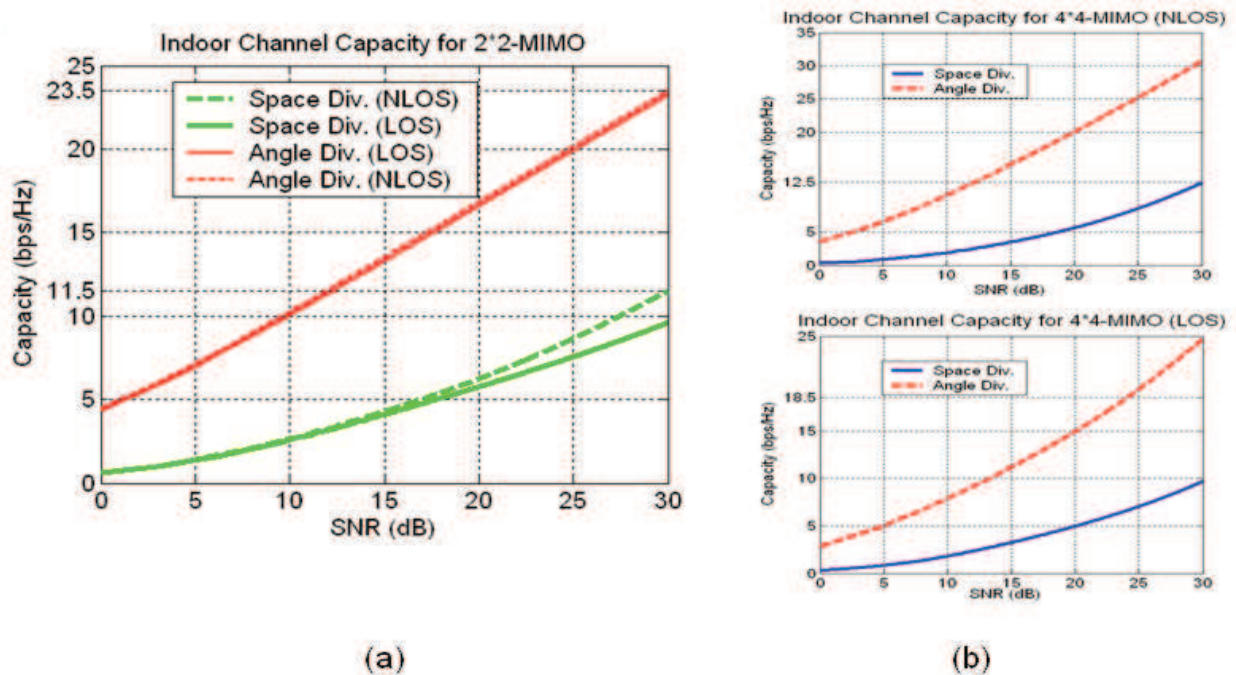

Fig. 19. Capacity for (a) 2×2-MIMO and (b) 4×4-MIMO systems.

	SV1	SV2	SV3	SV4
Space Div. (LOS) 4×4-MIMO	1.0000	0.0067	0.0008	0.0000
Angle Div. (LOS) 4×4-MIMO	1.0000	0.1120	0.0011	0.0005
Space Div. (NLOS) 4×4-MIMO	1.0000	0.0208	0.0087	0.0002
Angle Div. (NLOS) 4×4-MIMO	1.0000	0.2252	0.0658	0.0000
Space Div. (LOS) 2×2-MIMO	1.0000	0.0094	-------	-------
Angle Div. (LOS) 2×2-MIMO	1.0000	0.1529	-------	-------
Space Div. (NLOS) 2×2-MIMO	1.0000	0.0011	-------	-------
Angle Div. (NLOS) 2×2-MIMO	1.0000	0.1816	-------	-------

Table 8. Comparing singular values for the 2×2-MIMO and 4×4-MIMO systems (SV: Singular Value).

however, since no direct path exists, there is more freedom to find the desirable angles. Therefore, different angles for the NLOS case are chosen for beams that one of them is not that far from the horizontal plane.

In practical application, even though it would not be feasible to perform angle optimization every time there is a change in the Tx and Rx position, there is a possibility to develop a method for finding optimum angles. In the systems that reference signals are used even infrequently, the initial optimization based on these signals can be done and followed by updates by estimating the Angle of Arrival (AOA). The assumption in this work was that receiver has no information about the channel. This means beamforming methods that need temporal and spatial reference (training signals) is not applicable. In that case semi-blind adaptive beamforming techniques can be utilized to find the optimum angles [Allen & Ghavami, 2005]. Main concern in this work can be if the angle diversity with non-optimum angles can still outperform space diversity. Therefore, angles were chosen heuristically and no optimization was performed to find the best possible ones. The results show, for the 2×2-MIMO system similar to what was obtained for the 4×4-MIMO system, angle diversity works better for both LOS and NLOS cases. Although angle diversity for 4×4-MIMO system shows better performance, still 2×2-MIMO system gives desirable results. If one uses beamforming techniques more desirable results might be achieved.

Space and angle diversity methods are also compared for office area where scatterers are in cluster form. First beam angles were chosen based on the clusters' location and they were (61º, 77º, 103º, 121º). It can be noted that these beams are very close to each other and have some cusps. These cusps cause increase in the correlation among the channels and show decrease in channel capacity, therefore they were changed in such a way that have less cusp (43º, 73º, 108º, 136º), but they were not directed to clusters any more. This improved the capacity. The capacity results for both sets are given in Fig. 20. In general cluster location can give a good guide to find the beam angles and then by considering the cusps between beams and blockage by walls a correction should be applied to improve the capacity.
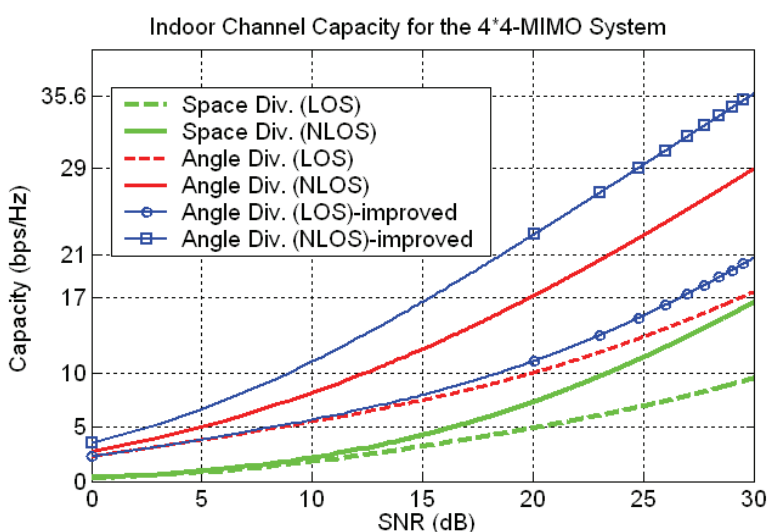

Fig. 20. Channel capacity for 30 scatterers in cluster form in the 4×4-MIMO system.

6. Conclusion

In this chapter a mathematical model to characterize wireless communication channel is developed which falls into semi-deterministic channel models. This model is based on electromagnetic scattering and reflecting and fundamental physics however it has been kept simple through appropriate assumptions.

Based on the results obtained from the SISTER model, impact of different factors on the channel capacity were studied for different scenarios which represent possible wireless MIMO systems such as Wireless Local Area Networks (WLAN) systems in real outdoor and indoor environments. Performance of space and angle diversity methods in MIMO systems are also compared and evaluated. Some of the main achievements are as follows.

The results obtained by SISTER model confirms that higher capacities are achieved for NLOS cases compare to LOS or quasi-LOS cases. However, in LOS or quasi-LOS cases where there is a single dominant path which introduces correlation among the MIMO channels, strong path's dominancy can be lessened by another strong path obtained from either a strong reflection or a resultant path of large number of scatterers and hence channel capacity will be improved. A better alternative to space diversity to improve the channel capacity (especially for LOS case) is the use of angle diversity method. This technique is a promising solution in MIMO systems whose main advantage is to allocate high capacity not to all the points but to the desired ones which results in minimum interference for undesired areas. Therefore, it can be very attractive for environments where interference is the main consideration. Probably the main advantage of angle diversity over space diversity is the similar performance of LOS and NLOS cases, while the space diversity shows a significant reduction in performance for the LOS case.

For angle diversity method in LOS case, high performance can be achieved by selecting beams such that they are not close to horizontal plane where usually a direct path exists. In fact, in LOS cases nulls of the beams should be directed towards the direct path between Tx and Rx to create decorrelated channels.

Even though angle diversity often shows better channel orthogonality, improperly chosen angles lessen the probability of obtaining the maximum achievable capacity. Therefore, choosing the right angles is very important. Improper selection can degrade the performance of a 4×4-MIMO system to that one of a 2×2-MIMO system. In general locations of clusters of scatterers can give a good guide to find the beam angles. However, after the initial selection correction has to be done to avoid beam cusps and blockage by walls. This is because the beam cusps can degrade the capacity due to increase correlation between channels. Based on this study, only in some scenarios, angle diversity shows better performance in LOS cases compare to NLOS as some scatterers which can be those with high contributions on channel orthogonality are blocked. Consequently, for most scenarios, angle diversity seems to be an appropriate alternative for space diversity which can provide similar orthogonality with less interference. Even if in some cases it shows less orthogonality still better performance than space diversity can be achieved because of higher SNR due to the array gain.

7. References

Allen, B. & Beach, M. (2004). On the analysis of switched beam antennas for the WCDMA downlink, *IEEE Trans. Veh. Technol.*, Vol. 53, No. 3, (2004), pp. 569-578.

Allen, B.; Brito, R.; Dohler, M. & Aghvami, H. (2004). Performance comparison of spatial diversity array technologies, *IEEE Trans. Consum. Electron.*, Vol. 50, No. 2, (2004), pp. 420-428.

Allen B. & Ghavami M. (2005). *Adaptive Array Systems: Fundamentals and Applications*, John Wiley & Sons, Inc., 978-0-470-86189-9, NY, USA.

Almers P.; Bonek E.; Burr A.; Czink, N.; Debbah M.; Degli-Esposti V.; Hofstetter H.; Kyosti P.; Laurenson D.; Matz G.; Molisch A. F.; Oestges C. & H. Ö̈ zcelik H. (2007). Survey of channel and radio propagation models for wireless MIMO systems, *EURASIP J. Wirel. Commun. Netw.*, pp. 1-19, (2007).

Anderson, C.R. & Rappaport, T.S. (2004). In-building wideband partition loss measurements at 2.5 and 60 GHz, *IEEE Trans. Wirel. Commun.* Vol. 3, No. 3, (2004), pp. 922 – 928.

Balanis, C. (1989). *Advanced Engineering Electromagnetics*, John Wiley & Sons, Inc., 0-471-621943, NY, USA.

Balanis, C. (1997). Antenna Theory Analysis and Design, John Wiley & Sons, Inc., 0-471-59268-4, NY, USA.

Burr, A. G. (2003). Capacity bounds and estimates for the finite scatterers MIMO Wireless Channel, *IEEE J. Sel. Areas Commun.*, Vol. 21, No. 5, (2003), pp. 812-818.

Chizhik, D.; Ling, J.; Wolniansky, P.W.; Valenzuela, R.A.; Costa, N. & Huber, K. (2003). Multiple-input-multiple-output measurements and modeling in Manhattan, *IEEE J. Sel. Areas Commun.*, 2003, Vol. 21, No. 3, (2003), pp. 321 – 331.

Collin, R.E. (1985). *Antennas and Radiowave Propagation*, McGraw-Hill, NY, USA.

E. Forooshani, A. (2006). *MIMO systems channel modeling and analysis*, Master of Science Thesis, University of Manitoba, Canada.

E. Forooshani, A. & Noghanian, S. (2010). Semi-deterministic channel model for MIMO systems Part-I: Model development and validation, *IET Microwave Antennas and Propag.*, Vol. 4, No. 1, (2010), pp. 17-25.

Foschini, J. & Gans, M. (1998). On the limit of wireless communications in a fading environment when using multiple antennas, *Wirel. Pers. Commun.*, Vol. 6, No. 3, (1998), pp. 311-335.

Gesbert, D.; Bolcskei, H.; Gore, D.A. & Paulraj, A.J. (2002). Outdoor MIMO wireless channels: models and performance prediction, *IEEE Trans. Commun.* , Vol. 50, No.12, (2002), pp. 1926 – 1934.

Howard, S.; Inanoglu, H.; Ketchum, J.; Wallace, M. & Walton, R. (2002). Results from MIMO channel measurements, *Proc. 13th IEEE Symp. Personal Indoor and Mobile Radio Communications,* pp. 1932 – 1936, Lisboa, Portugal, Sept. 2002.

Liberti, J.C. & Rappaport, T.S. (1996). A geometrically based model for line-of-sight multipath radio channels, *Proc. IEEE 46th, Vehicular Technology Conf.*, pp. 844 – 848, Atlanta, GA, 1996.

Liberti J.C. & Rappapaort, T.S. (1999). *Smart Antennas for Wireless Communications*, Prentice Hall, 0137192878, Upper Saddle River, NJ, USA.

Ranvier, S.; Kivinen, J. & Vainikainen, (2007). Millimeter-wave MIMO radio channel sounder, *IEEE Trans. Instrum. Meas.*, Vol. 56, No. 3, (2007), pp. 1018 – 1024.

Remcom Inc. Technical Staff (2004). *Wireless Insite*, Remcom Inc., version 2.0.5.

Seidel, S.Y. & Rappaport, T.S. (1994). Site-specific propagation prediction for wireless in-building personal communication system design, *IEEE Trans. Veh. Technol.*, Vol. 43, No.4, (1994), pp. 879 – 891.

Svantesson, T. (2001). *Antenna and Propagation from a Signal Processing Perspective*, PhD dissertation, Chalmers University of Technology, Sweden.

Wentworth, S.M. (2005). *Fundamentals of Electromagnetics with Engineering Applications*, John Wiley & Sons, 978-0-470-10575-7, 111 River Street, Hoboken, NJ, USA.

MIMO Systems, Theory and Applications

Edited by Dr. Hossein Khaleghi Bizaki

In recent years, it was realized that the MIMO communication systems seems to be inevitable in accelerated evolution of high data rates applications due to their potential to dramatically increase the spectral efficiency and simultaneously sending individual information to the corresponding users in wireless systems. This book, intends to provide highlights of the current research topics in the field of MIMO system, to offer a snapshot of the recent advances and major issues faced today by the researchers in the MIMO related areas. The book is written by specialists working in universities and research centers all over the world to cover the fundamental principles and main advanced topics on high data rates wireless communications systems over MIMO channels. Moreover, the book has the advantage of providing a collection of applications that are completely independent and self-contained; thus, the interested reader can choose any chapter and skip to another without losing continuity.

How to reference

In order to correctly reference this scholarly work, feel free to copy and paste the following:

Arghavan Emami-Forooshani and Sima Noghanian (2011). Semi-Deterministic Single Interaction MIMO Channel Model, MIMO Systems, Theory and Applications, Dr. Hossein Khaleghi Bizaki (Ed.), ISBN: 978-953-307-245-6, InTech, Available from: http://www.intechopen.com/books/mimo-systems-theory-and-applications/semi-deterministic-single-interaction-mimo-channel-model

INTECH
open science | open minds